THE JOURNAL OF PHYSICAL CHEMISTRY C

Article

Cite This: J. Phys. Chem. C 2019, 123, 14089−14096

pubs.acs.org/JPCC

Charge Density Wave State Suppresses Ferromagnetic Ordering in VSe_2 Monolayers

Paula Mariel Coelho,[†] Kien Nguyen Cong,[†] Manuel Bonilla,[†] Sadhu Kolekar,[†] Manh-Huong Phan,[†] José Avila,[‡,§] Maria C. Asensio,[‡,§,∥] Ivan I. Oleynik,[†] and Matthias Batzill*[,†]

[†]Department of Physics, University of South Florida, Tampa, Florida 33620, United States

[‡]L'Orme des Merisiers, Synchrotron SOLEIL, Saint Aubin-BP 48, Gif sur Yvette Cedex 91192, France

[§]L'Orme des Merisiers, Université Paris-Saclay, Saint Aubin-BP 48, Gif sur Yvette, Cedex 91192, France

[∥]Madrid Institute of Materials Science (ICMM), Spanish Scientific Research Council (CSIC), Cantoblanco, E-28049 Madrid, Spain

Supporting Information

ABSTRACT: Ferromagnetic ordering of monolayer vanadium dichalcogenides (VSe_2 and VS_2) has been predicted by density functional theory (DFT), and suggestive experimental evidence for magnetic ordering in VSe_2 monolayers has been reported. However, such ferromagnetic ordering would be in stark contradiction to the known paramagnetic nature of the bulk VSe_2. Herein, we investigate the electronic structure of VSe_2 monolayers by angle-resolved photoemission spectroscopy (ARPES) and first-principles DFT. The ARPES measurements demonstrate the absence of spin-polarized bands for monolayers in close correspondence to nonmagnetic nature of the bulk VSe_2. We demonstrate that the stabilization of the nonmagnetic state occurs due to the appearance of a charge density wave (CDW) state in VSe_2 monolayers. In contrast to well-established $4 \times 4 \times 3$ periodicity of the CDW in bulk VSe_2, we identify a $\sqrt{3} \times \sqrt{7}$ unit cell for VSe_2 monolayers from both scanning tunneling microscopy imaging and first-principles calculations. Moreover, DFT predicts that the $\sqrt{3} \times \sqrt{7}$ charge order state is energetically competitive with a ferromagnetic 1×1 state. This suggests that the experimentally observed CDW state is the nonmagnetic ground state of a *perfect* VSe_2 monolayer, consistent with the absence of spin-polarized bands in ARPES measurements. Therefore, monolayer VSe_2 is not an itinerant magnet.

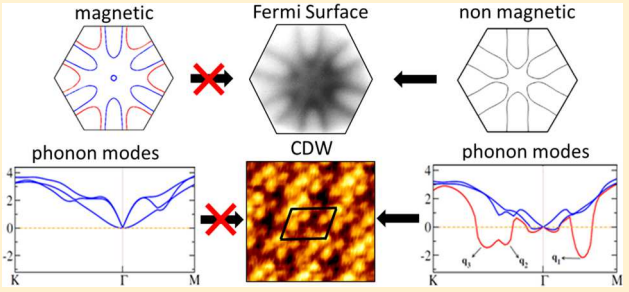

1. INTRODUCTION

Monolayer van der Waals materials exhibiting ferromagnetic ordering are attractive candidates for novel van der Waals heterostructure devices, where magnetic proximity effects combined with weak chemical interactions may be exploited to design new functionalities. Such heterostructures may be fabricated either by mechanical exfoliation and stacking or by direct growth methods.[1,2] Recently, it has been shown that van der Waals materials displaying ferromagnetic ordering in the bulk can be reduced to a single ferromagnetic layer.[3,4] It has been also demonstrated that the magnetic properties of such ultrathin materials can be tuned by external electric fields[5] and van der Waals heterostructures can exhibit magnetoresistance.[6,7] As most of these materials possess low Curie temperature below room temperature,[3,4,8] they are not suitable for practical applications. Therefore, there is an urgent need to develop new van der Waals materials exhibiting ferromagnetic ordering close to room temperature.[9,10]

Numerous density functional theory (DFT) calculations have consistently predicted ferromagnetic ordering in the family of simple vanadium dichalcogenides, i.e., VX_2 with X = S, Se, or Te, with high Curie temperatures.[11−22] These predictions are controversial as standard DFT often faces challenges in reproducing the experimental lattice parameters and predicts the H-structure to be favored over the experimentally observed 1T-phase.[13] Importantly, DFT also regularly fails to reproduce the paramagnetic nature of the bulk phases of these materials observed in experiment,[23,24] although taking the presence of the charge density wave (CDW) in bulk VSe_2 may resolve some discrepancy between experiments and DFT for bulk VSe_2.[25] CDW order was also observed in misfit layer compounds and ferecrystals, in which VSe_2 layers are sandwiched in between rocksalt-type monochalcogenides; however, no magnetism was reported for these materials.[26,27] Nevertheless, experimental evidence of magnetism was found in VSe_2 monolayer/few-layer materials either produced by liquid exfoliation[28] or grown in single-layer form,[29] which makes the issue of ferromagnetic ordering in single-layer VSe_2 worth investigating further.

Here, we perform a combined angle-resolved photoemission spectroscopy (ARPES) and DFT study of epitaxial VSe_2

Received: May 6, 2019
Published: May 13, 2019

DOI: 10.1021/acs.jpcc.9b04281
J. Phys. Chem. C 2019, 123, 14089−14096

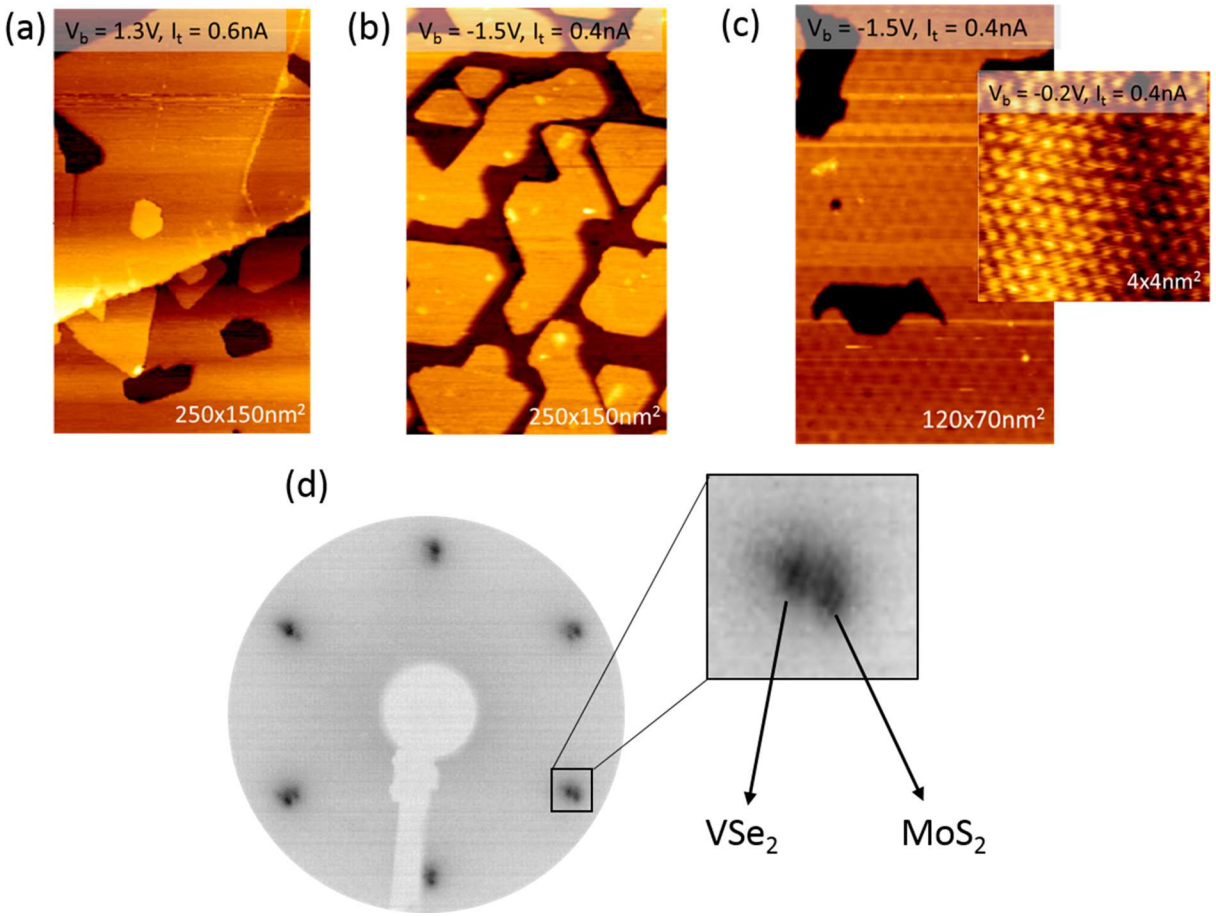

Figure 1. MBE grown VSe_2 monolayer samples. Large-scale STM images of monolayer islands of VSe_2 on (a) HOPG and (b) MoS_2. In (c) the moiré structure of VSe_2 on the MoS_2 substrate is visible while the inset shows the hexagonal atomic corrugation. The LEED pattern of submonolayer VSe_2 on MoS_2 is shown in (d). The diffraction spots for VSe_2 align perfectly with those of the MoS_2 substrate, indicating the van der Waals epitaxy (i.e., rotational alignment) of the VSe_2 layer with the substrate.

monolayers to complement previous experimental studies of ferromagnetism by looking for signatures of spin-polarized effects in the band structure. In clear conflict with DFT predictions, no spin split bands are observed in ARPES,[30−33] thus questioning the existence of itinerant ferromagnetism in monolayer VSe_2. This apparent discrepancy is resolved by predicting and observing the CDW state of monolayer VSe_2. Both low-temperature scanning tunneling microscopy (STM) and DFT simulations show that VSe_2 exhibits a lattice distortion induced by CDW resulting in a nonmagnetic ground state for monolayer VSe_2 consistent with the absence of spin split bands and recent X-ray magnetic circular dichroism experiments.[31,33] Consequently, rather than being an intrinsic property of monolayer VSe_2, the experimentally observed ferromagnetism in MBE grown samples[29] must originate from other factors. Thus, the main contribution of this work is to trace the origin of the numerous erroneous DFT predictions of a ferromagnetic ground state to the fact that these studies did not consider the actual CDW ground state.

2. METHODS

2.1. Experimental Methods. Monolayer samples were grown by molecular beam epitaxy (MBE) on single crystalline MoS_2, $MoTe_2$, HOPG, or hex-BN substrates. The substrates were cleaved in air and immediately introduced in the UHV chamber. Before growth the substrates were degassed for 6 h in UHV at 325 °C. Monolayer films were grown at a very low growth rate of ∼1 ML in 80 min by codeposition of V and Se at substrate growth temperature of ∼300 °C. Vanadium was evaporated from a high-purity 2 mm diameter rod in a water-cooled e-beam evaporator while atomic Se was supplied from a hot wall Se-cracker source. After growth the samples were transferred from the growth chamber into a surface analysis chamber equipped for X-ray photoemission spectroscopy (XPS), ultraviolet photoemission spectroscopy (UPS), and STM. STM measurements were taken on selective samples at room temperature and at 80 K with electrochemically etched tungsten tips, cleaned in the STM by voltage pulsing. Additional STM characterization was performed in a separate STM cooled to ∼20 K by a closed-cycle cryostat. The samples were transferred from the growth chamber to the low-temperature STM in a vacuum suitcase without exposure to air. Other samples were protected with ∼10 nm Se capping layer by depositing Se in the MBE chamber at room temperature. Such protected samples could be transported through air for characterization with other instruments. VSe_2 monolayers on MoS_2 substrates were packed in an argon-filled container and shipped to the French synchrotron SOLEIL for ARPES characterization at the ANTARES beamline. After insertion into the preparation chambers the samples were decapped by annealing in UHV to ∼250 °C. The cleanliness of the samples was evident from the absence of oxygen and only a

DOI: 10.1021/acs.jpcc.9b04281
J. Phys. Chem. C 2019, 123, 14089−14096

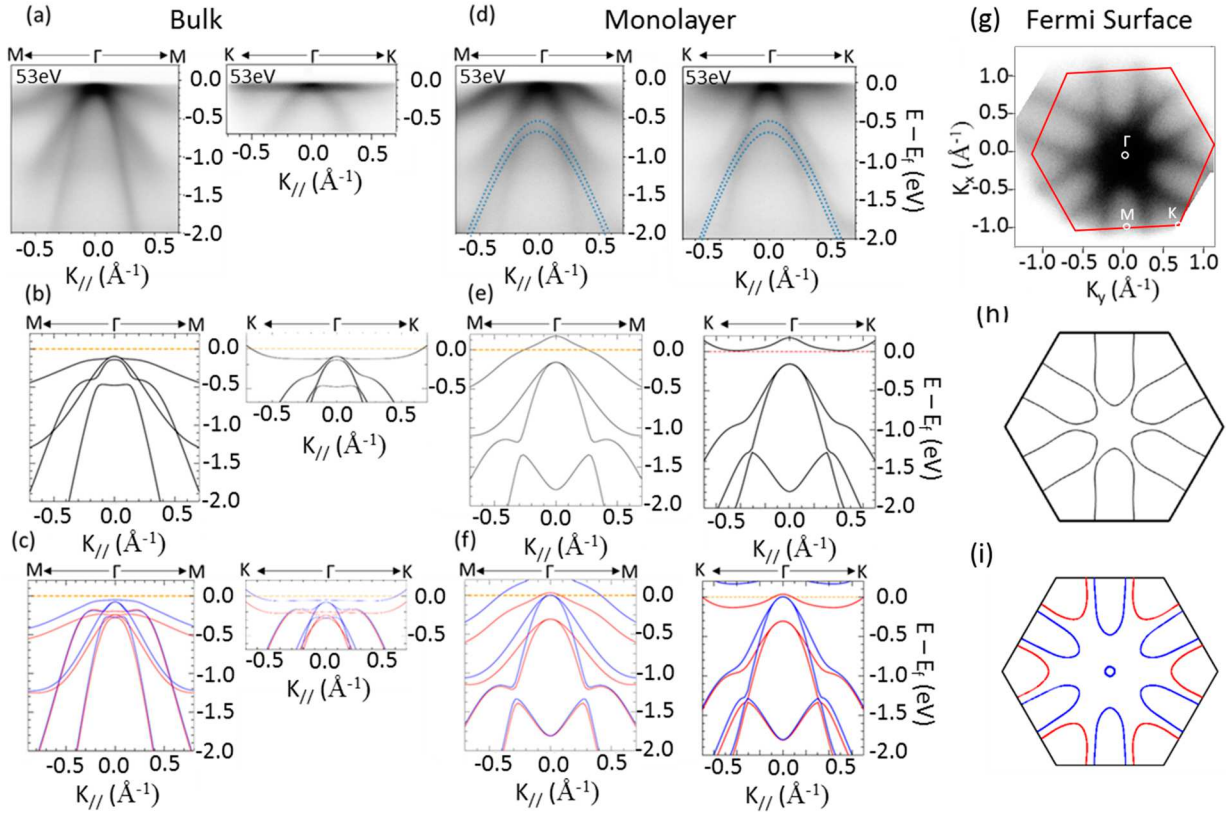

Figure 2. ARPES and band structure calculations for monolayer and surface of bulk VSe_2. The ARPES spectra for bulk VSe_2 surface along Γ−M and Γ−K directions are shown in (a) and are compared to non-spin-polarized and spin-polarized DFT calculations shown in (b) and (c), respectively. The corresponding ARPES for monolayer VSe_2 is shown in (d). The bands originating from the MoS_2 substrate are indicated as dashed lines in (d). Non-spin-polarized and spin-polarized DFT simulations for monolayer VSe_2 are shown in (e) and (f), respectively. The measured Fermi surface for the monolayer is shown in (g), and calculated non-spin-polarized and spin-polarized Fermi surfaces are shown in (h) and (i). The experiment clearly displays a lack of spin-split bands, in apparent contradiction to spin-polarized calculations. In contrast, the experimental results are in good agreement with non-spin-polarized calculations. All the experiments shown here are acquired with 53 eV photon energy.

very small carbon peak in soft X-ray core-level spectra with $h\nu$ = 700 eV. The ANTARES beamline is optimized for ARPES and nanospot ARPES. In this study we did not need nanometric lateral resolution, and we just used regular ARPES with a spot size of ∼120 μm. This is possible because of the excellent epitaxial relationship between the grown VSe_2 films and the single crystalline MoS_2 substrate, as is also evident from low-energy electron diffraction (LEED). The angular and energy resolution of the ANTARES beamline are ∼0.2° and ∼10 meV, respectively. In addition to monolayer samples we also investigated surfaces of bulk 1T-VSe_2 single crystals, commercially available from Graphene HQ. These single crystals were cleaved in UHV before measurements. All ARPES measurements were taken with the sample temperature around 100 K.

2.2. Computational Methods. The DFT calculations of electronic and atomic structure were performed using the Vienna Ab-initio Simulation Package (VASP)[34] employing projector augmented wave (PAW)[35] potentials; the plane wave energy cutoff was 500 eV, and very dense *k*-point grids of 11 × 11 × 1 for 1T structures and for 5 × 7 × 1 for CDW structures and 0.001 eV/ Å force tolerance during optimization of the atomic positions were used. Although various functionals have been investigated, the local density approximation (LDA)[36] was chosen for production calculations based on the best agreement with available experimental data (see the Supporting Information for more details). The Fermi surface calculations of the normal state-1T structure were done using superdense *k*-point grid of 41 × 41 × 5. The Fermi surfaces are visualized using Xcrysden[37] software. Phonon calculations are performed using the linear response method implemented in Quantum Espresso[38] (QE) code. QE phonon calculations employed energy cutoff of 50 Ry, while the phonon Brillouin zone was sampled with 11 × 11 × 1 *q*-points in the case of 1T structure. The evolutionary crystal structure prediction of monolayer VSe_2 was performed vy using USPEX code[45−47] interfaced with VASP using up to 36 atoms/unitcell.

3. RESULTS AND DISCUSSION

VSe_2 (sub)monolayer samples were grown on HOPG or synthetically grown MoS_2 single crystals. Figure 1 shows STM images of VSe_2 grown on HOPG and MoS_2. VSe_2 grows more uniformly on MoS_2 while on HOPG it preferentially grows along step edges. On MoS_2, good monolayer growth can be achieved. Monolayer VSe_2 on MoS_2 exhibits a pronounced moiré structure while on graphite the moiré structure is much weaker. This may indicate stronger interactions of VSe_2 with MoS_2 than HOPG. Only hexagonal structures are observed in atomic resolution images at room temperature. LEED patterns of VSe_2 on single crystalline MoS_2 substrates are shown in Figure 1d for VSe_2. Both the MoS_2 substrate diffraction spots and those of the monolayer are seen, illustrating the alignment

DOI: 10.1021/acs.jpcc.9b04281
J. Phys. Chem. C 2019, 123, 14089−14096

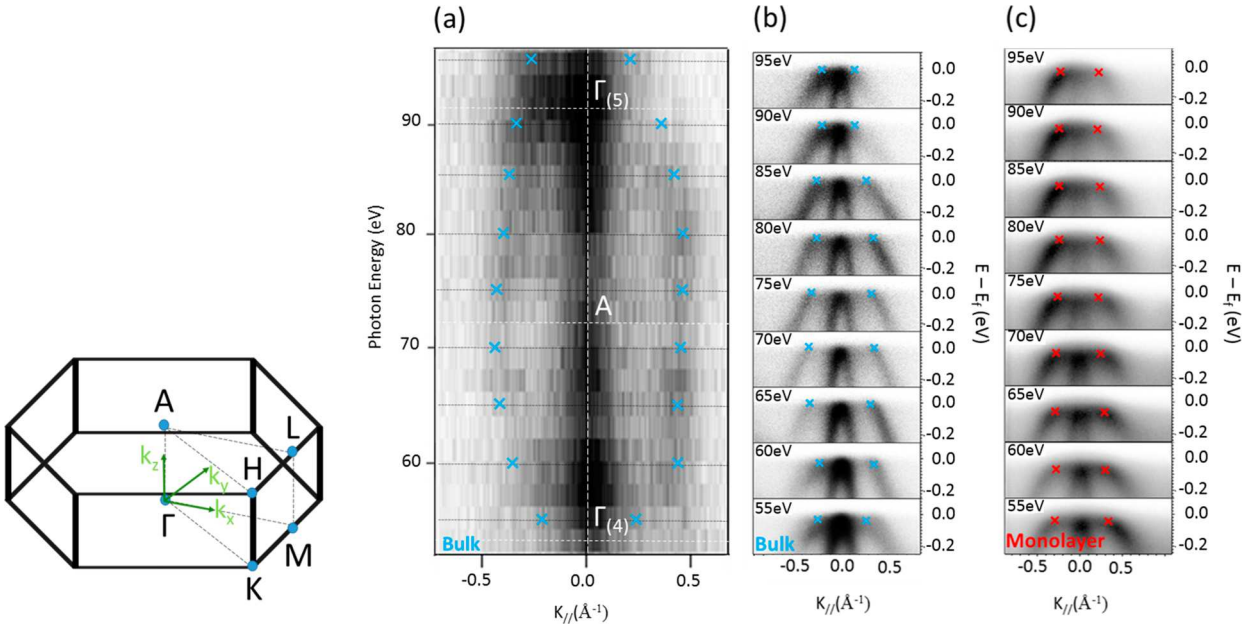

Figure 3. Band dispersion in the Γ−A direction for the bulk VSe_2 surface measured by varying the photon energy between 55 and 95 eV. The Fermi surface of the bulk sample in the Γ−A direction is shown in (a). The photoemission intensity at the Γ-point is dominated by the Se-4p band that just touches the Fermi level. The V-3d band of the bulk sample shows a dispersion with photon energy, which is indicated with blue crosses. This is also seen in (b) which shows spectra along the Γ−M (A−L) direction. The intersection of the V-3d band with the Fermi level is indicated by blue crosses in (b), and it has the same dispersion as shown in (a). In contrast, for monolayer samples the intersection of the V-3d band with the Fermi level is independent of the photon energy, indicated by red crosses in (c) and illustrating the 2D nature of the monolayer. This difference in the dispersion along the k_z direction is the only discernible difference in the electronic structure of the monolayer compared to bulk VSe_2.

of the monolayer with the substrate, which makes it suitable for ARPES measurements. Surprisingly, as we have reported previously, all these samples show well-pronounced ferromagnetic response with a large magnetization in a magnetometer.[29] A similar strong magnetic response was also reported for VSe_2 grown on graphene/SiC samples.[30] Importantly, the measured magnetization appears to result in unphysically large magnetic moments per atom if assumed they originate from VSe_2 alone.

3.1. Electronic Structure Measurements of VSe_2 by ARPES. The electronic structure of VSe_2 has been measured by ARPES at the ANTARES beamline of the SOLEIL synchrotron. Both epitaxial monolayer VSe_2 on MoS_2 substrates and in situ cleaved VSe_2 single crystal samples were studied to allow direct comparison between monolayer samples and bulk surfaces.

Figure 2 shows the band dispersions along the Γ−X and Γ−M directions for the VSe_2 bulk crystal (Figure 2a) and the VSe_2 monolayer grown on a MoS_2 single crystal substrate (Figure 2d). The MoS_2 substrate contributes a weak feature (indicated in Figure 2d by dashed lines) which must not be attributed to VSe_2 bands. Careful direct comparison of the spectra for monolayer and bulk shows that there are only very small differences in the case of the monolayer samples. Any difference between the bulk and monolayer can, in fact, be explained by the previously reported weak interlayer interactions in the bulk VSe_2, which cause a dispersion in the normal k_z direction[39] of the Brillouin zone. Such dispersion is naturally absent in the case of a perfect 2D monolayer. Specifically, for this particular photon energy, there is a small difference in the k_{II} at which the V d-band intersects the Fermi surface in the Γ−M direction, with the monolayer intersecting the Fermi level at slightly larger k_{II} than that for the bulk sample. Such variations are, however, expected for bands that disperse in the k_z direction. In fact, measuring the dispersion of the bulk material along k_z, by varying the photon energy, we observe the variation of the k_{II} intersection of the V d-band with the Fermi surface (see Figure 3). As expected, only the bulk sample shows a dispersion normal to the surface. Consequently, the only differences in the band structure of bulk and monolayer VSe_2 arise from a weak k_z dispersion of the bands in bulk samples. Otherwise, their band structures are almost identical. This fact specifically indicates that the monolayer does not exhibit any itinerant magnetic state, since bulk VSe_2 is known to be paramagnetic.

To provide a more detailed interpretation of the ARPES results, we perform DFT band structure calculations of single layer and bulk VSe_2. The experimental measurements are reasonably well described by non-spin-polarized DFT band structure shown in Figures 2b and 2e for bulk and monolayer samples, respectively. In contrast, the spin-polarized DFT calculation indicates the formation of additional spin-split minority and majority bands as shown in Figures 2c and 2f. The minority band would give rise to a hole pocket at the Fermi surface around the M-point, which is clearly absent in the experimental Fermi surface (additional constant energy surfaces are shown in Figure S1). Therefore, there exists no evidence for the existence of such split bands in the experimental ARPES studies. Moreover, the non-spin-polarized DFT band structure calculations for bulk and monolayers are in good agreement with experiment, thus confirming that the monolayer VSe_2 is nonmagnetic.

It is also noteworthy that standard DFT (at both LDA and GGA levels) also predicts a ferromagnetic state of the *bulk* VSe_2. The spin-polarized bands for the bulk samples display, however, a much smaller splitting compared to that of the single layer (see Figure 2c). The prediction of ferromagnetism

DOI: 10.1021/acs.jpcc.9b04281
J. Phys. Chem. C 2019, 123, 14089−14096

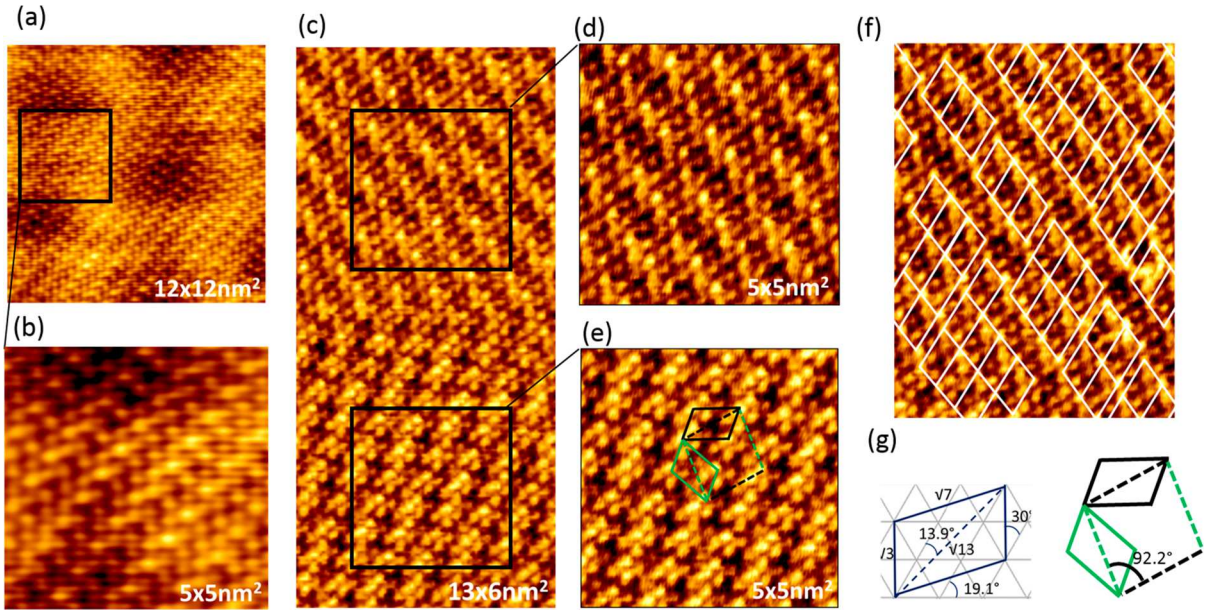

Figure 4. Low-temperature STM images of CDW order in monolayer VSe_2. On the MoS_2 substrate the CDW is superimposed on the moiré structures (a, b). Different rotational domains are observed (c), and the unit cell can be identified as a $\sqrt{3}R30 \times \sqrt{7}R19.1$ superstructure with respect to the VSe_2 unit cell. The same structure can be described by two mirrored unit cells as illustrated in (e). An alternative unit cell is that described by the unit-cell diagonals of the two mirrored primitive unit cells as illustrated in (g). Often antiphase domain boundaries are observed in the CDW structure as shown in (f), giving rise to only small domains.

of VSe_2 is in apparent contradiction with well-established experimental observation of the paramagnetic nature of bulk VSe_2 even at very low temperatures. In addition, DFT faces a difficulty in predicting relative stability of two possible phases of a single layer of VSe_2. Depending on the specific density functional employed in calculations, either the 1T or 2H phase is stable. However, the ARPES data clearly show that 1T is the phase observed in experiment because these two phases have very different electronic properties. Specifically, the semimetallic nature of the 2H phase predicted by DFT[20] is not observed in our ARPES experiments on MBE grown monolayer samples. This apparent disagreement of DFT results with experiment prompts more thorough DFT investigation (see section 3.3).

3.2. Charge Density Wave State of Monolayer VSe_2. One possible source of contradictory DFT prediction of a ferromagnetic ground state for both bulk and single layer VSe_2 is the existence of competing states, e.g., the CDW state which is known to exist in the case of the bulk VSe_2 at temperatures below ~110 K. Therefore, it seems plausible that the similar CDW lattice distortion of perfect 1T structure of single layer VSe_2 may lower the energy of the system, resulting in stabilization of thus possibly stabilizing the nonmagnetic phase. Therefore, the important question is whether CDW state also exists for monolayers of VSe_2, and if it does, could it suppress a ferromagnetic ordering?

STM studies at low temperatures (20−80 K) display a superstructure (see Figure 4), which we interpret as a CDW order. It is known that the bulk and few-layer VSe_2 undergo a CDW transition displaying a 4 × 4 periodicity in the basal plane,[40] which has been explained by Fermi surface nesting. In the bulk the nesting vector was suggested to be three-dimensional, requiring the warping of the Fermi surface in the k_z direction normal to the basal planes.[39,41] In the case of the monolayer, no dispersion in the k_z direction exists. Consequently, a different nesting condition should exist, resulting in a different charge order state compared to the bulk. Recently, a variation of the charge order transition temperature has been observed for VSe_2 upon reduction of its thickness;[28,42] however, its reported nonmonotonic dependence is puzzling.[40] In the bulk, the transition temperature is around 110 K. Our STM data do not allow us to determine accurately the transition temperature for the monolayer samples, but measurements at up to 80 K suggest that the CDW does exist at least up to this temperature. We also observe the same periodicities of CDW structures of VSe_2 monolayer on both HOPG and MoS_2 substrates, indicating that the kind of van der Waals substrate does not influence significantly the charge order state. As pointed out above, the monolayer VSe_2 on MoS_2 substrate exhibits an additional moiré structure even at room temperature; therefore, the atomic configuration of the charge order state is superimposed on that of the moiré pattern. Importantly, while bulk VSe_2 exhibits a 4 × 4 CDW, the CDW observed for the monolayer is more complex and has a lower symmetry, giving rise to rotational domains in STM.[43] The primitive unit cell identified in STM images is $\sqrt{3}R30 \times \sqrt{7}R19.1$ (see Figure 4e). The long diagonal of this unit cell has a length of $\sqrt{13}a_{Vse2}$, which is rotated by 13.9° with respect to the low index direction. It is noteworthy that this unit cell has two mirror-symmetric variations, with their corresponding diagonals rotated by 92.2°, resulting in a nonprimitive unit cell with $\sqrt{13}a_{Vse2}$ cell vectors as illustrated in Figure 4g. The identification of the unit cell is complicated by the fact that even at 20 K only small domains are observed, which are interrupted by antiphase domain boundaries as shown in Figure 4f. This may indicate that slightly different charge order states compete or that the system is close to an incommensurate CDW.

To investigate whether the observed real space charge order state can be explained by a Fermi surface nesting condition, we use the Fermi surface measured for the monolayer sample (see Figure 5). The d-electrons of vanadium form pockets around

DOI: 10.1021/acs.jpcc.9b04281
J. Phys. Chem. C 2019, 123, 14089−14096

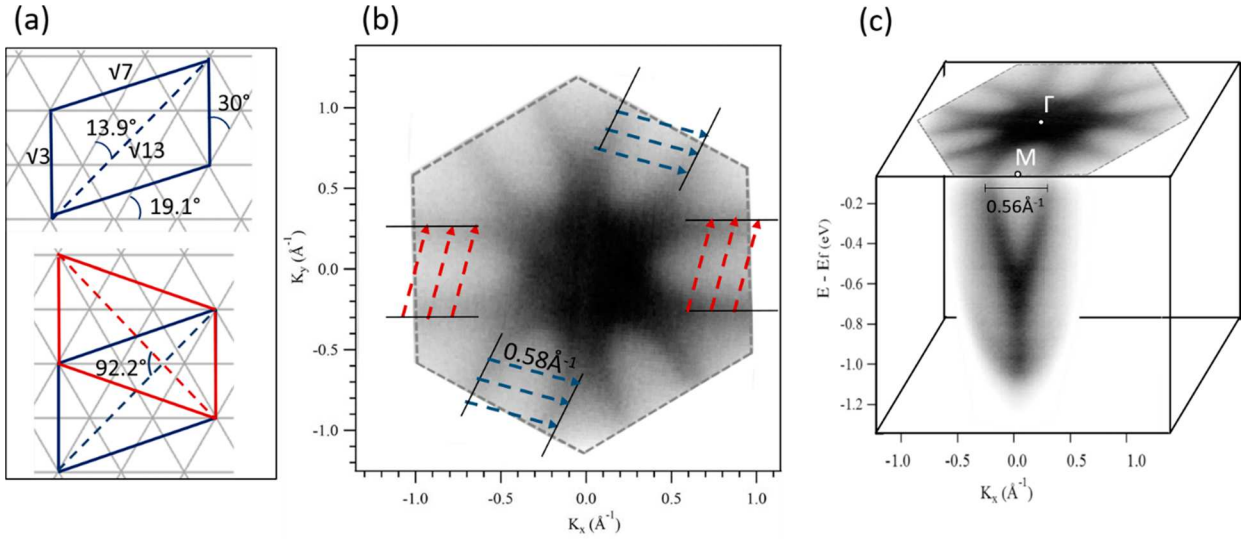

Figure 5. Fermi surface nesting condition. The Fermi surface of VSe_2 consists of parallel sheets of the V-3d pockets at the Brillouin zone boundary with a separation of 0.56 $Å^{-1}$ shown in (c). The reciprocal vector of the diagonal of the primitive CDW unit cell describes a nesting vector that can translate one Fermi sheet onto the other as shown in (b). Thus, the observed CDW fulfills a Fermi nesting condition.

the M-points with extended parallel Fermi sheets. This suggests excellent nesting condition: one Fermi sheet can be translated onto the other with a single translation vector. At the BZ boundary we measure a separation of the intersect of the V d-band with the Fermi level of k = 0.56 $Å^{-1}$ across the M-point as illustrated in Figure 5c. The corresponding real space vector (oriented in the $R30$ direction) does not match the lattice periodicity and thus cannot form a commensurate CDW. Consequently, slightly rotated nesting conditions need to be explored. Assuming a commensurate CDW, only a few discrete reciprocal lattice vectors are allowed to describe a nesting vector for our Fermi surface. A list of allowed reciprocal vectors corresponding to a commensurate real space vector and their nesting conditions are given in the Supporting Information (see Figure S2). The closest commensurate nesting vector is indeed the $\sqrt{13}R13.9°$, consistent with the observed real space unit cell as indicated in Figure 5. Consequently, Fermi surface nesting appears to describe the CDW order surprisingly well despite the deficiencies of the Fermi nesting model.[44] A more solid interpretation of a CDW instability comes from ab initio calculations, which is discussed next.

3.3. First-Principles Calculations of Charge Density Wave Structure of Monolayer VSe_2. To gain insight into the nature of the CDW state, we perform a DFT investigation of its atomic structure. First, the stability analysis of perfect monolayer VSe_2 is performed by calculating its phonon spectrum and examining whether there are modes with imaginary phonon frequencies. We then use first-principles evolutionary crystal structure prediction to uncover its atomic structure. The spin-restricted DFT calculations of the phonon spectrum do find phonon modes with imaginary frequencies (see Figure 6a), including the one close to the middle point along the Γ−M direction of the BZ and two others along the Γ−K direction. We find that the wavevector $\mathbf{q}_3 \sim (-0.2, 0.4)$ at the minimum is commensurate with the $\sqrt{3}R30 \times \sqrt{7}R19$ superstructure observed in the experiment. Interestingly, the phonon dispersion from spin-polarized calculations does not exhibit imaginary phonon modes, as shown in Figure 6b, thus

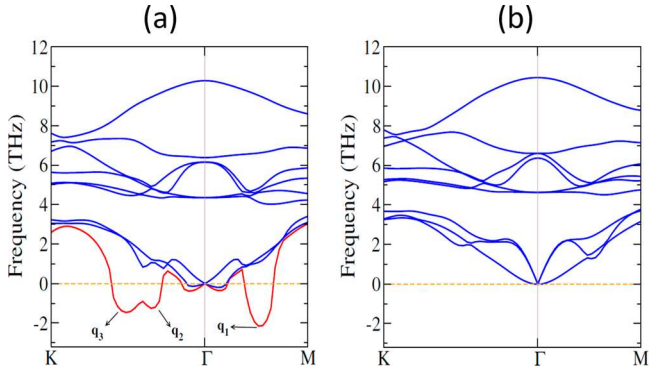

Figure 6. Calculated phonon band structure of 1T monolayer structure of VSe_2 (a) using spin-restricted DFT and (b) using spin-polarized DFT. The phonon soft modes with imaginary frequencies are highlighted by red color.

demonstrating a competition between the CDW state and magnetism.

To determine the positions of the atoms in the lowest energy CDW structure of monolayer VSe_2, we displace atoms along the $\mathbf{q}_3$ wave vector and then relax their positions. We find that the energy of the resultant $\sqrt{3}R30 \times \sqrt{7}R19.1$ CDW modulated structure is ∼8 meV/atom lower than that of the initial 1 × 1 unit cell of the perfect VSe_2. Importantly, this nonmagnetic CDW structure is ∼4 meV/atom lower than that of the undistorted lattice in ferromagnetic state, displaying a substantial preference for the CDW lattice.

To independently verify this finding, we search for lowest energy structure of the VSe_2 monolayer using the first-principles evolutionary crystal structure prediction method USPEX[45−47] with no prior input other than the stoichiometry and the shape of 2D unit cell. The search easily finds the $\sqrt{3}R30 \times \sqrt{7}R19.1$ CDW crystal, thus clearly demonstrating the energetic preference of the CDW state. As illustrated in Figure 7, the simulated STM image of the CDW modulated structure is in a good agreement with experiment, thus providing further validation of the theoretical predictions. The

DOI: 10.1021/acs.jpcc.9b04281
J. Phys. Chem. C 2019, 123, 14089−14096

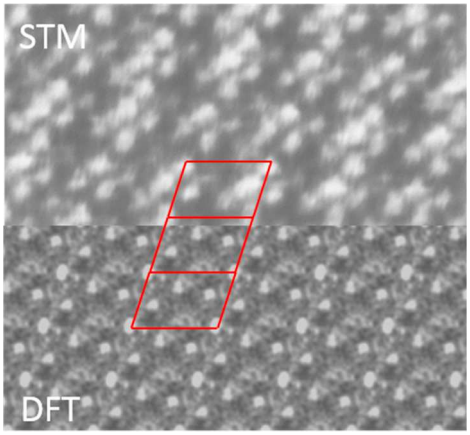

Figure 7. Comparison between experimental STM images of the CDW state in monolayer VSe_2 (top) with simulated STM image of the predicted CDW structure (bottom). The agreement, apart from a broadening of the structure in the experiment, is excellent, confirming the correct simulated CDW structure.

crystal structure of the CDW unit cell is reported in a cif file included in the Supporting Information.

4. CONCLUSIONS

This work demonstrates that the previous DFT predictions of band magnetism in monolayer VSe_2 are erroneous. The comparative ARPES studies of monolayer and bulk samples show similar electronic properties for both systems, thus displaying no evidence of spin splitting of bands. Moreover, we find that while a 4×4 CDW modulation of the basal planes is observed in bulk samples, the monolayer exhibits a more complex $\sqrt{3}R30 \times \sqrt{7}R19.1$ unit cell. This CDW structure is also predicted by first-principles crystal structure searching. The difference between monolayer and bulk might originate from the lack of a third dimension of the Fermi surface in the case of the monolayer samples, and thus it can be attributed to the effect of dimensionality. Our DFT calculations indicate a competition between the CDW state and ferromagnetic ordering in VSe_2. They also confirm that nonmagnetic charge ordered state is the ground state of the VSe_2 monolayer, in agreement with ARPES measurements which display the lack of spin splitting of the band structure. This apparent absence of itinerant magnetism in VSe_2 monolayers may also caution other DFT predictions of magnetism in metallic 2D materials and illustrates the importance of competing ground states, particularly CDW states, for determining the properties of this class of materials.

■ ASSOCIATED CONTENT

Supporting Information

The Supporting Information is available free of charge on the ACS Publications website at DOI: 10.1021/acs.jpcc.9b04281.

Constant binding energy surfaces; relation of commensurate real space vectors to reciprocal space nesting vectors (PDF)

Crystallographic data for the predicted CDW unit cell (CIF)

■ AUTHOR INFORMATION

Corresponding Author

*E-mail mbatzill@usf.edu.

ORCID

Ivan I. Oleynik: 0000-0002-5348-6484

Matthias Batzill: 0000-0001-8984-8427

Author Contributions

P.M.C. and K.N.C. contributed equally to this work.

Notes

The authors declare no competing financial interest.

■ ACKNOWLEDGMENTS

Financial support from the National Science Foundation through Award DMR-1701390 is acknowledged.

■ REFERENCES

(1) Gong, C.; Zhang, X. Two-Dimensional Magnetic Crystals and Emergent Heterostructure Devices. *Science* **2019**, *363*, eaav4450.

(2) Liu, S.; Yuan, X.; Zou, Y.; Sheng, Y.; Huang, C.; Zhang, E.; Ling, J.; Liu, Y.; Wang, W.; Zhang, C.; Zou, J.; Wang, K.; Xiu, F.; et al. Wafer-Scale Two-Dimensional Ferromagnetic Fe_3GeTe_2 Thin Films Grown by Molecular Beam Epitaxy. *npj 2D Mater. Appl.* **2017**, *1*, 30.

(3) Huang, B.; Clark, G.; Navarro-Moratalla, E.; Klein, D. R.; Cheng, R.; Seyler, K. L.; Zhong, D.; Schmidgall, E.; McGuire, M. A.; Cobden, D. H.; et al. Layer-Dependent Ferromagnetism in a Van Der Waals Crystal down to the Monolayer Limit. *Nature* **2017**, *546*, 270−273.

(4) Gong, C.; Li, L.; Li, Z.; Ji, H.; Stern, A.; Xia, Y.; Cao, T.; Bao, W.; Wang, C.; Wang, Y.; et al. Discovery of Intrinsic Ferromagnetism in Two-Dimensional Van Der Waals Crystals. *Nature* **2017**, *546*, 265−269.

(5) Huang, B.; Clark, G.; Klein, D. R.; MacNeill, D.; Navarro-Moratalla, E.; Seyler, K. L.; Wilson, N.; McGuire, M. A.; Cobden, D. H.; Xiao, D.; et al. Electrical Control of 2D Magnetism in Bilayer CrI_3. *Nat. Nanotechnol.* **2018**, *13*, 544−548.

(6) Klein, D. R.; MacNeill, D.; Lado, J. L.; Soriano, D.; Navarro-Moratalla, E.; Watanabe, K.; Taniguchi, T.; Manni, S.; Canfield, P.; Fernández-Rossier, J.; et al. Probing Magnetism in 2D Van Der Waals Crystalline Insulators via Electron Tunneling. *Science* **2018**, *360*, 1218−1222.

(7) Song, T.; Cai, X.; Tu, M.W.-Y.X.; Huang, B.; Wilson, N. P.; Seyler, K. L.; Zhu, L.; Taniguchi, T.; Watanabe, K.; McGuire, M. A.; et al. Giant Tunneling Magnetoresistance in Spin-Filter Van Der Waals Heterostructures. *Science* **2018**, *360*, 1214−1218.

(8) Deiseroth, H.-J.; Aleksandrov, K.; Reiner, C.; Kienle, L.; Kremer, R. K. Fe3GeTe2 and Ni3GeTe2− Two New Layered Transition-Metal Compounds: Crystal Structures, HRTEM Investigations, and Magnetic and Electrical Properties. *Eur. J. Inorg. Chem.* **2006**, *8*, 1561−1567.

(9) Deng, Y.; Yu, Y.; Song, Y.; Zhang, J.; Wang, N. Z.; Sun, Z.; Yi, Y.; Wu, Y. Z.; Wu, S.; Zhu, J.; et al. Gate-Tunable Room-Temperature Ferromagnetism in Two-Dimensional Fe_3GeTe_2. *Nature* **2018**, *563*, 94−99.

(10) May, A. F.; Ovchinnikov, D.; Zheng, Q.; Hermann, R.; Calder, S.; Huang, B.; Fei, Z.; Liu, Y.; Xu, X.; McGuire, M. A. Ferromagnetism Near Room Temperature in the Cleavable van der Waals Crystal Fe_5GeTe_2. *ACS Nano* **2019**, *13*, 4436−4442.

(11) Ma, Y.; Dai, Y.; Guo, M.; Niu, C.; Zhu, Y.; Huang, B. Evidence of the Existence of Magnetism in Pristine VX_2 Monolayers (X = S, Se) and Their Strain-Induced Tunable Magnetic Properties. *ACS Nano* **2012**, *6*, 1695−1701.

(12) Zhuang, H. L.; Hennig, R. G. Stability and Magnetism of Strongly Correlated Single-Layer VS_2. *Phys. Rev. B: Condens. Matter Mater. Phys.* **2016**, *93*, 054429.

(13) Esters, M.; Hennig, R. G.; Johnson, D. C. Dynamic Instabilities in Strongly Correlated VSe_2 Monolayers and Bilayers. *Phys. Rev. B: Condens. Matter Mater. Phys.* **2017**, *96*, 235147.

(14) Pan, H. Magnetic and Electronic Evolutions of Hydrogenated VTe_2 Monolayer under Tension. *Sci. Rep.* **2015**, *4*, 7524.

(15) Zhang, H.; Liu, L. M.; Lau, W. M. Dimension-Dependent Phase Transition and Magnetic Properties of VS_2. *J. Mater. Chem. A* **2013**, *1*, 10821−10828.
(16) Gao, D.; Xue, Q.; Mao, X.; Wang, W.; Xu, Q.; Xue, D. Ferromagnetism in Ultrathin VS_2 Nanosheets. *J. Mater. Chem. C* **2013**, *1*, 5909−5916.
(17) Pan, H. Electronic and Magnetic Properties of Vanadium Dichalcogenides Monolayers Tuned by Hydrogenation. *J. Phys. Chem. C* **2014**, *118*, 13248−13253.
(18) Manchanda, P.; Skomski, R. 2D Transition-Metal Diselenides: Phase Segregation, Electronic Structure, and Magnetism. *J. Phys.: Condens. Matter* **2016**, *28*, 064002.
(19) Wasey, A. H. M. A.; Chakrabarty, S.; Das, G. P. Quantum Size Effects in Layered VX_2 (X = S, Se) Materials: Manifestation of Metal to Semimetal or Semiconductor Transition. *J. Appl. Phys.* **2015**, *117*, 064313.
(20) Tong, W.-Y.; Gong, S.-J.; Wan, X.; Duan, C.-G. Concepts of Ferrovalley Material and Anomalous Valley Hall Effect. *Nat. Commun.* **2016**, *7*, 13612.
(21) Du, J.; Xia, C.; Xiong, W.; Wang, T.; Jia, Y.; Li, J. Two-Dimensional Transition-Metal Dichalcogenides-Based Ferromagnetic Van Der Waals Heterostructures. *Nanoscale* **2017**, *9*, 17585.
(22) Fuh, H.-R.; Chang, C.-R.; Wang, Y.-K.; Evans, R. F. L.; Chantrell, R. W.; Jeng, H.-T. New Type Single-Layer Magnetic Semiconductor in Transition-Metal Dichalcogenides VX_2 (X = S, Se and Te). *Sci. Rep.* **2016**, *6*, 32625.
(23) Bayard, M.; Sienko, M. J. Anomalous Electric and Magnetic Properties of Vanadium Diselenide. *J. Solid State Chem.* **1976**, *19*, 325−329.
(24) van Bruggen, C. F.; Haas, C. Magnetic Susceptibility and Electrical Properties of VSe_2 Single Crystals. *Solid State Commun.* **1976**, *20*, 251−254.
(25) Fumega, A. O.; Pardo, V. Absence of Ferromagnetism in VSe_2 Caused by its Charge Density Wave State. arXiv:1804.07102.
(26) Falmbigl, M.; Putzky, D.; Ditto, J.; Esters, M.; Bauers, S. R.; Ronning, F.; Johnson, D. C. Influence of Defects on the Charge Density Wave of $([SnSe]_{1+\delta})_1(VSe_2)_1$ Ferecrystals. *ACS Nano* **2015**, *9*, 8440−8448.
(27) Falmbigl, M.; Fiedler, A.; Atkins, R. E.; Fischer, S. F.; Johnson, D. C. Suppressing a Charge Density Wave by Changing Dimensionality in the Ferecrystalline Compounds $([SnSe]_{1.15})_1(VSe_2)$n with n = 1, 2, 3, 4. *Nano Lett.* **2015**, *15*, 943−948.
(28) Xu, K.; Chen, P.; Li, X.; Wu, C.; Guo, Y.; Zhao, J.; Wu, X.; Xie, Y. Ultrathin Nanosheets of Vanadium Diselenide: A Metallic Two-Dimensional Material with Ferromagnetic Charge-Density-Wave Behavior. *Angew. Chem., Int. Ed.* **2013**, *52*, 10477−10481.
(29) Bonilla, M.; Kolekar, S.; Ma, Y.; Diaz, H. C.; Kalappattil, V.; Das, R.; Eggers, T.; Gutierrez, H. R.; Phan, M.-H.; Batzill, M. Strong Room Temperature Ferromagnetism in VSe_2 Monolayers on Van Der Waals Substrates. *Nat. Nanotechnol.* **2018**, *13*, 289−203.
(30) Duvjir, G.; Choi, B. K.; Jang, I.; Ulstrup, S.; Kang, S.; Ly, T. T.; Kim, S.; Choi, Y. H.; Jozwiak, C.; Bostwick, A.; et al. Emergence of a Metal−Insulator Transition and High-Temperature Charge-Density Waves in VSe_2 at the Monolayer Limit. *Nano Lett.* **2018**, *18*, 5432−5438.
(31) Feng, J.; Biswas, D.; Rajan, A.; Watson, M. D.; Mazzola, F.; Clark, O. J.; Underwood, K.; Marković, I.; McLaren, M.; Hunter, A.; et al. Electronic Structure and Enhanced Charge-Density Wave Order of Monolayer VSe_2. *Nano Lett.* **2018**, *18*, 4493−4499.
(32) Chen, P.; Pai, W. W.; Chan, Y.-H.; Madhavan, V.; Chou, M. Y.; Mo, S.-K.; Fedorov, A.-V.; Chiang, T.-C. Unique Gap Structure and Symmetry of the Charge Density Wave in Single-Layer VSe_2. *Phys. Rev. Lett.* **2018**, *121*, 196402.
(33) Wong, P. K. J.; Zhang, W.; Bussolotti, F.; Yin, X.; Herng, T. S.; Zhang, L.; Huang, Y. L.; Vinai, G.; Krishnamurthi, S.; Bukhvalov, D. W.; et al. Evidence of Spin Frustration in a Vanadium Diselenide Monolayer Magnet. *Adv. Mater.* **2019**, 1901185.
(34) Kresse, G.; Furthmüller, J. Efficiency of Ab-Initio Total Energy Calculations for Metals and Semiconductors Using a Plane-Wave Basis Set. *Comput. Mater. Sci.* **1996**, *6*, 15−50.
(35) Blöchl, P. E. Projector Augmented Wave Method. *Phys. Rev. B: Condens. Matter Mater. Phys.* **1994**, *50*, 17953−17979.
(36) Ceperley, D. M.; Alder, B. J. Ground State of the Electron Gas by a Stochastic Model. *Phys. Rev. Lett.* **1980**, *45*, 566−569.
(37) Kokalj, A. XCrySDen—A New Program for Displaying Crystalline Structures and Electron Densities. *J. Mol. Graphics Modell.* **1999**, *17*, 176−179.
(38) Giannozzi, P.; Baroni, S.; Bonini, N.; Calandra, M.; Car, R.; Cavazzoni, C.; Ceresoli, D.; Chiarotti, G. L.; Cococcioni, M.; Dabo, I.; et al. QUANTUM ESPRESSO: A Modular and Open-Source Software Project for Quantum Simulations of Materials. *J. Phys.: Condens. Matter* **2009**, *21*, 395502.
(39) Strocov, V. N.; Shi, M.; Kobayashi, M.; Monney, C.; Wang, X.; Krempasky, J.; Schmitt, T.; Patthey, L.; Berger, H.; Blaha, P. Three-Dimensional Electron Realm in VSe_2 by Soft-X-Ray Photoelectron Spectroscopy: Origin of Charge-Density Waves. *Phys. Rev. Lett.* **2012**, *109*, 086401.
(40) Pasztor, A.; Scarfato, A.; Barreteau, C.; Giannini, E.; Renner, C. Dimensional Crossover of the Charge Density Wave Transition in Thin Exfoliated VSe_2. *2D Mater.* **2017**, *4*, 041005.
(41) Tsutsumi, K. X-Ray-Diffraction Study of the Periodic Lattice Distortion Associated with a Charge-Density Wave in 1T-VSe_2. *Phys. Rev. B: Condens. Matter Mater. Phys.* **1982**, *26*, 5756−5759.
(42) Yang, J. Y.; Wang, W.; Liu, Y.; Du, H.; Ning, W.; Zheng, G.; Jin, C.; Han, Y.; Wang, N.; Yang, Z.; et al. Thickness Dependence of the Charge-Density-Wave Transition Temperature in VSe_2. *Appl. Phys. Lett.* **2014**, *105*, 063109.
(43) Liu, Z.-L.; Wu, X.; Shao, Y.; Qi, J.; Cao, Y.; Huang, L.; Liu, C.; Wang, J.-O.; Zheng, Q.; Zhu, Z.-L.; et al. Epitaxially Grown Monolayer VSe_2: An Air-stable Magnetic Two-dimensional Material with Low Work Function at Edges. *Sci. Bulletin* **2018**, *63*, 419−425.
(44) Johannes, M. D.; Mazin, I. I. Fermi Surface Nesting and the Origin of Charge Density Waves in Metals. *Phys. Rev. B: Condens. Matter Mater. Phys.* **2008**, *77*, 165135.
(45) Oganov, A. R.; Glass, C. W. Crystal Structure Prediction Using Ab Initio Evolutionary Techniques: Principles and Applications. *J. Chem. Phys.* **2006**, *124*, 244704.
(46) Glass, C. W.; Oganov, A. R.; Hansen, N. USPEX: Evolutionary Crystal Structure Prediction. *Comput. Phys. Commun.* **2006**, *175*, 713−720.
(47) Lyakhov, A. O.; Oganov, A. R.; Valle, M. How to Predict Very Large and Complex Crystal Structures. *Comput. Phys. Commun.* **2010**, *181*, 1623−1632.

DOI: 10.1021/acs.jpcc.9b04281
J. Phys. Chem. C 2019, 123, 14089−14096